Helical Microfiber Bragg Grating Printed by Femtosecond Laser for Refractive Index Sensing

Changrui Liao, Kaiming Yang, Jia Wang, Zhiyong Bai, Zongsong Gan, and Yiping Wang, *Senior Member, IEEE*

***Abstract*— A microfiber helical Bragg grating is demonstrated for use in refractive index measurements. The proposed sensor was fabricated using a femtosecond laser-induced multiphoton polymerization technique. The grating was cured along with the microfiber, and its reflection spectra, transmission spectra, refractive index, and temperature cross sensitivity were investigated. The refractive index sensitivities of ∼229 and ∼120 nm/RIU were achieved, corresponding to high order and fundamental modes, respectively. This helical microfiber Bragg grating exhibits high refractive index sensitivity and good mechanical strength and could potentially be used for optical functionality integration.**

***Index Terms*— Fiber Bragg gratings, fiber optic sensors, microstructure fabrication.**

I. Introduction

FEMTOSECOND (Fs) lasers have been utilized in a variety of micro- and nano-machining techniques, to solve problems in a diverse range of scientific and industrial fields. Recently, additive manufacturing methods, based on Fs laser-induced multiphoton polymerization (MPP), have attracted increased attention due to their ultra-precise spatial and temporal control of photochemical reactions. As such, they have been widely used in the nanostructure fabrication of microfluidic chips, photonic crystals, and micro-electromechanical systems (MEMS) [1]–[5]. Due to multiphoton absorption, fabrication resolution is not restricted to the diffraction limit but is determined instead by the intensity of the focused Fs laser beam. Additionally, focusing the beam in the photoresist confines multiphoton absorption to the focal point, enabling 3D microfabrication. This process can be used for the integration of functional micro-devices such as lab-on-fiber systems.

Microfibers, defined as having a diameter of less than 10 μm, allow transmitted light to interact strongly with the surrounding medium via large evanescent fields [6]. Microfiber Bragg gratings (μ-FBGs) provide a useful sensing configuration, successfully fabricated using various techniques. These have included Fs laser micromachining [7], [8], ultraviolet (UV) laser irradiation [9], and focused ion beam (FIB) milling [10]. Each of these methods induce periodic refractive index (RI) modulation inside the microfiber. The primary advantage of this approach is high efficiency for exciting Bragg resonance. However, it also reduces device mechanical strength as the fiber structure is compromised. In a previous study, we proposed Fs laser-induced MPP for μ-FBG fabrication [11]. This method provides significant manufacturing flexibility but the grating structure is unstable because of limited contact area between the printed grating segments and the microfiber.

In this study, a helical μ-FBG was successfully fabricated by Fs laser-induced MPP. Compared with previously reported polymerized μ-FBGs, this helical μ-FBG exhibits better spectral quality and improved mechanical strength due to enhanced contact area between the printed grating and the microfiber. The polymerized grating acts as a protective jacket that makes the device more stable. The helical μ-FBG also provides good RI response across a range of 1.345 to 1.395, with sensitivities of ∼229 nm/RIU and ∼120 nm/RIU for high-order and fundamental modes, respectively. These values are higher than previously reported μ-FBGs, ranging from 30 nm/RIU to 207 nm/RIU [12]–[14]. This helical μ-FBG could have potential applications in microfluidic systems and the proposed Fs laser 3D microprinting method offers a powerful tool for constructing new optical fiber sensors.

II. Device Design and Fabrication

A schematic diagram of Fs laser microprinting of helical μ-FBGs is shown in Fig. 1(a). The grey region denotes a tapered microfiber and the yellow region identifies the polymerized helical grating structure. In this experiment, a microfiber was tapered from a single mode fiber (SMF-28)

Manuscript received January 25, 2019; revised March 19, 2019; accepted March 20, 2019. Date of publication April 23, 2019; date of current version June 3, 2019. This work was supported in part by the National Natural Science Foundation of China (NSFC) under Grant 61575128, in part by the Natural Science Foundation of Guangdong Province under Grant 2018B030306003, in part by the Science and Technology Innovation Commission of Shenzhen under Grant KQJSCX20170727101953680, and in part by the Development and Reform Commission of the Shenzhen Municipality Foundation. *(Corresponding author: Yiping Wang.)*

C. Liao, K. Yang, J. Wang, Z. Bai, and Y. Wang are with the Guangdong and Hong Kong Joint Research Centre for Optical Fibre Sensors, Shenzhen University, Shenzhen 518060, China, and also with the Key Laboratory of Optoelectronic Devices and Systems of Ministry of Education and Guangdong Province, College of Optoelectronic Engineering, Shenzhen University, Shenzhen 518060, China (e-mail: cliao@szu.edu.cn; yangkaiming@email.szu.edu.cn; wangjia2016@email.szu.edu.cn; baizhiyong@szu.edu.cn; ypwang@szu.edu.cn).

Z. Gan is with the Wuhan National Laboratory for Optoelectronics (WNLO), Huazhong University of Science and Technology (HUST), Wuhan 430074, China (e-mail: ganzongsong@hust.edu.cn).

Color versions of one or more of the figures in this letter are available online at http://ieeexplore.ieee.org.

Digital Object Identifier 10.1109/LPT.2019.2912634

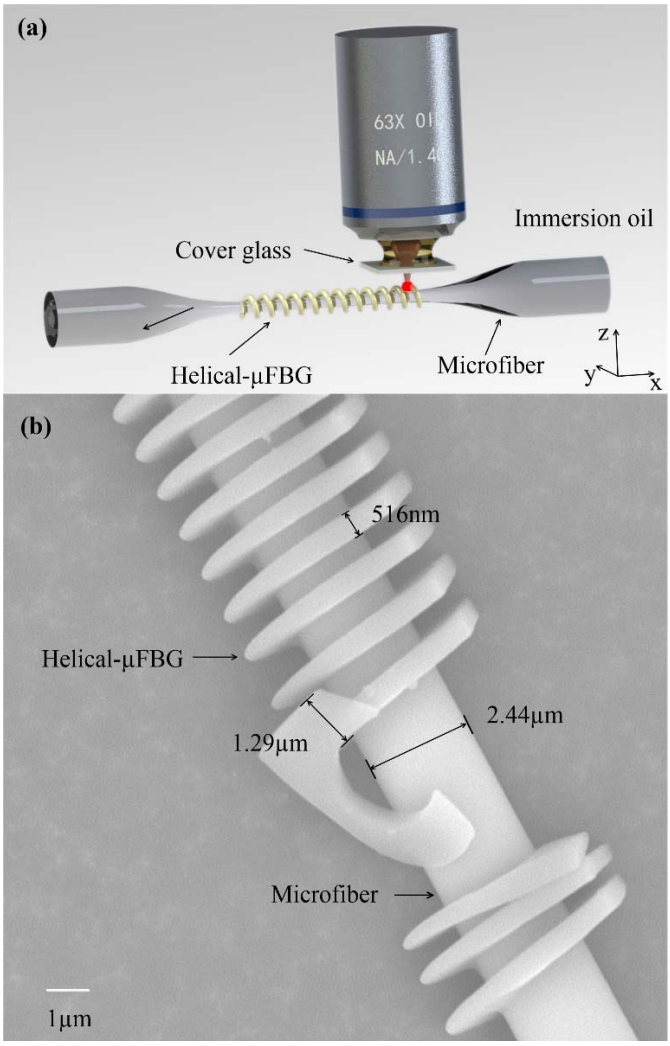

Fig. 1. (a) A schematic diagram of Fs laser microprinting of the helical μ-FBG. (b) The helical μ-FBG with a helical grating segment peeled away and exposed.

with a flame-heated drawing technique [15]. A microfiber with a diameter less than 2 μm has poor mechanical strength and is easily broken. In contrast, the evanescent field in the microfiber will weaken as the diameter increases, which results in weak surface modulations. As such, a microfiber diameter ranging from 2 μm to 3.5 μm was selected to achieve a balance between evanescent field and mechanical strength.

A unique liquid photoresin with strong mechanical properties was investigated in this study. The photoresin used in this work was prepared as follows. A photo-initiator (IGR-369, Ciba-Geigy) with a molar ratio of 2.5% and a trifunctional monomer SR444 (Pentaerythritol Triacrylate, Sartomer, Figure 1) with a molar ratio of 40% were introduced to keep the viscosity from decreasing the photoinhibition efficiency. SR368, a trifunctional monomer (Tris 2-Hydroxy Ethyl Isocyanurate Triacrylate, Sartomer,Figure 1) with a molar ratio of 30% was used to improve the chemical reactivity. This ensured high photosensitivity and mechanical strength and resisted both damage and shrinkage during the development process. SR454, another trifunctional monomer (Ethoxylated3 Trimethylolpropa-ne Triacrylate, Sartomer, Figure 1)

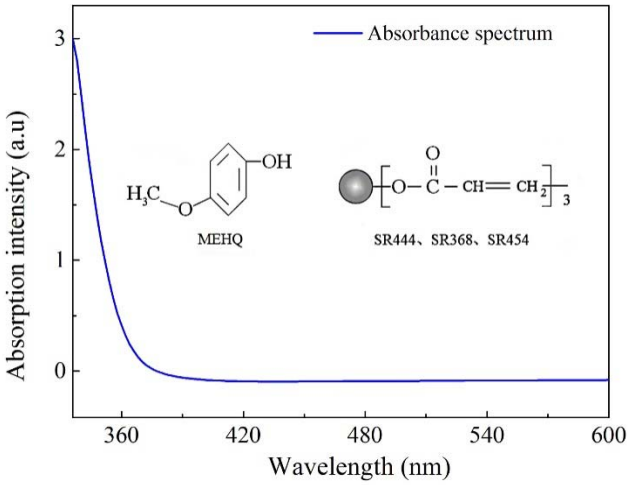

Fig. 2. The single-photon absorbance spectrum for the photoresin. The monomers used in this photoresin included SR368, which was used to improve the chemical reactivity, SR444, which was introduced to prevent the viscosity from decreasing the photoinhibition efficiency, and SR454, which was used to enhance mechanical strength.

with a molar ratio of 25% was used to improve the mechanical strength. These materials were first mixed and dissolved in acetone. The mixture was heated to 50°C and maintained for 1 hour to ensure sufficient dissolution. 4-Hydroxyanisole (MEHQ, Sigma Aldrich, Saint Louis, Missouri, USA, Figure 1) was used as a polymerization inhibitor and was added to the mixture at a molar ratio of 0.5%. After the complete dissolution of MEHQ, the mixture was heated to 120°C. Tetraethylthiuram disulphide (TED, Sigma Aldrich) with a molar ratio of 2.0% was adopted as an accelerator promoter. The mixture was maintained at 120°C for 10 minutes. A centrifuge was used to remove any undissolved chemicals. The resulting photoresin was then heated at 60°C for 1 hour. Figure 2 shows the single-photon absorbance spectrum for this photoresin.

An Fs laser (PHAROS, 1026 nm, 250 Fs, 200 kHz) and an oil-immersed objective lens with a numerical aperture (NA) of 1.4 were used in the laser printing process. The beam was tightly focused in the photoresist to initiate photochemical reactions at the focal point, inducing the cross-linking of monomers through radical polymerization [16]. The machined microfiber immersed in the photoresin was then mounted on a 3D air-bearing stage (Aerotech). The helical scanning trail was designed in the software. During fabrication, the beam was first focused on the edge of the microfiber surface and the helical grating structure was then polymerized using a preset scanning trail. The laser focal point was fixed and the microfiber mounted on the stage was translated along a circular pattern in the y-z plane, which transited a straight line along the x-axis. Polymerization time was ~10 minutes. Afterwards, the fiber was immersed in an acetone and isopropyl mixture (1:3) for 1 minute, to remove any non-polymerized photoresin. The RI of the polymerized photoresist was ~1.53 at 1550 nm. Fig. 1(b) shows a scanning electron microscope (SEM) image of the helical μ-FBG, with one piece of the helical grating segment peeled away using a tungsten probe. As seen in the figure, the diameter of the microfiber was 2.44 μm.

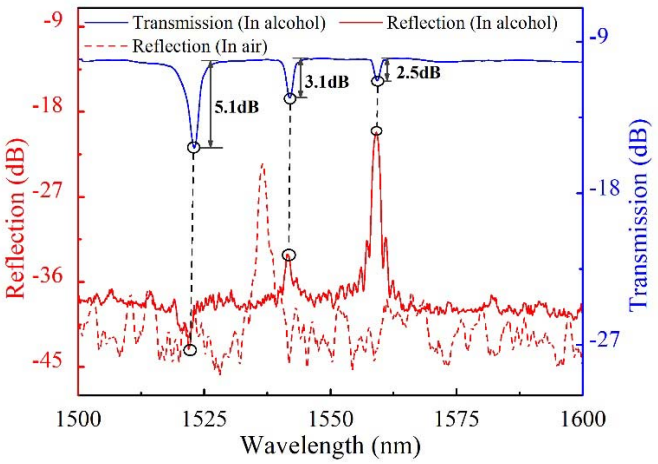

Fig. 3. The reflection and transmission spectra of the helical μ-FBG with a microfiber diameter of 3.5 μm. The red dotted line denotes the reflection spectrum in air. The red and blue lines denote the reflection and transmission spectra in alcohol, respectively.

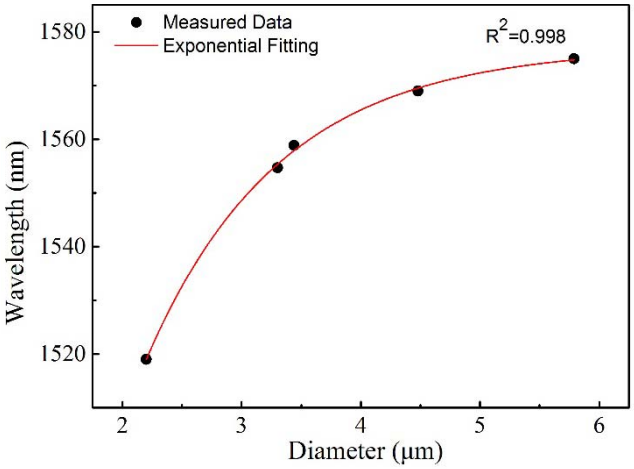

Fig. 4. The relationship between fundamental mode resonant wavelength and microfiber diameter.

The width and thickness of the grating segment were 516 nm and 1.29 μm, respectively.

III. Results and Discussion

The reflection and transmission spectra for the helical μ-FBG, with a microfiber diameter of 3.5 μm, were measured using a broadband light source (BBS) and an optical spectrum analyzer (OSA) with a resolution of 0.01 nm. The red dotted line in Fig. 3 denotes the reflection spectrum in air. The red and blue lines denote the reflection and transmission spectra in alcohol, respectively. The reflection spectrum experienced a significant red shift as the helical μ-FBG was immersed in alcohol (from air). This can be explained by an increased microfiber mode RI in the ambient medium. There are three significant Bragg resonances in the blue transmission spectrum (1559.3 nm/2.5 dB, 1542.0 nm/3.1 dB, 1523.0 nm/5.1 dB), which can be explained by the reflected fundamental mode and two high-order modes being coupled from forward fundamental modes. High-order modes showed higher excitation efficiency than fundamental modes, which may be the result of fiber-surface structural modulations in the helical μ-FBG. Abnormally, the reflectivity of high-order modes was much weaker than fundamental modes in the reflection spectrum (red line) because most of the light energy in high-order modes was filtered by the connected single mode fiber.

The effect of microfiber diameter on resonant wavelength was experimentally investigated and the fundamental mode was recorded. During fabrication, a Fs laser with a power of 1 mw and a fabrication speed of 30 μm/s was utilized to cure the helical grating. The grating featured a pitch of 1.1 μm and a pitch number of 500 for 5 microfibers with diameters ranging from 2.2 μm to 5.8 μm. The relationship between fundamental mode resonant wavelength and microfiber diameter is shown in Fig. 4, where the black points indicate measured resonance wavelength and the red line denotes an exponential fit. It can be seen from this figure that resonance shifts toward longer wavelengths as the microfiber diameter increases.

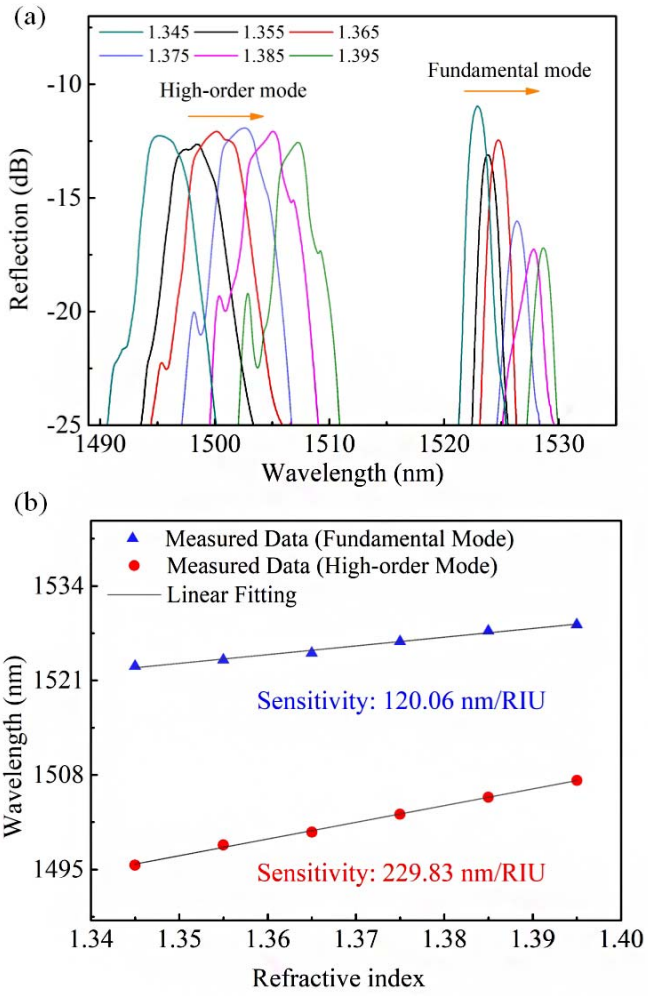

Fig. 5. (a) The reflection spectral evolution of the helical μ-FBG in liquids of varying RI. (b) The linear relationship between the Bragg resonance wavelength for the fundamental and high-order modes and ambient RI.

This is because thicker microfibers have a higher fundamental mode effective RI.

The ambient RI response for the helical μ-FBG was investigated at room temperature (22°C). A helical grating with a fiber diameter of 3.7 μm, a grating pitch of 1.07 μm,

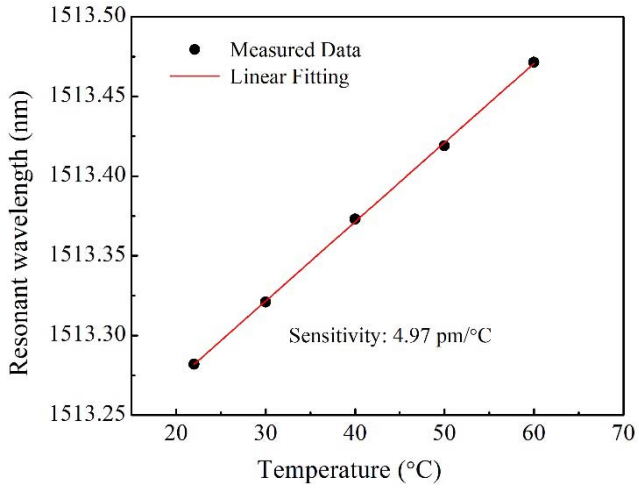

Fig. 6. The cross sensitivity of temperature for the helical μ-FBG as the temperature increased from 22°C to 60°C.

and a pitch number of 500 was used in the RI experiment. During the measurement process, the device was sequentially immersed in a series of RI liquids (Cargille Lab) whose RI values increased from 1.345 to 1.395 with a step size of 0.01. The device was carefully cleaned with alcohol after each test until no residual liquid remained, as verified by the restoration of the original spectrum. Fig. 5(a) demonstrates the reflection spectral evolution of the device in various liquids with RI values of 1.345, 1.355, 1.365, 1.375, 1.385, and 1.395. Both the fundamental mode and a high-order mode were traced. The relationship between Bragg resonance wavelength and liquid RI is shown in Fig. 5(b), where the Bragg wavelength of the fundamental and high-order modes are shown to vary linearly with ambient RI. The high-order mode exhibits a higher RI sensitivity (229 nm/RIU) than the fundamental mode (120 nm/RIU) over an RI range from 1.345 to 1.395. The improved RI response of the high-order mode results from larger evanescent fields.

The effect of temperature cross sensitivity on Bragg resonance wavelength was investigated in the helical μ-FBG by placing the device in an electric oven and gradually increasing the air temperature from 22°C to 60°C. A helical grating with a fiber diameter of 3.6 μm, a grating pitch of 1.08 μm, and a pitch number of 500 was employed in the temperature experiment. The results of this test are plotted in Fig. 6, where the μ-FBG resonance wavelength exhibits a linear relationship with ambient temperature. The temperature sensitivity was measured to be 4.97 pm/°C, which is similar to that of conventional FBGs [17].

IV. Conclusion

In this study, a helical μ-FBG fabricated by Fs laser-induced MPP was proposed and demonstrated. The helical grating structure was polymerized using a circular-scanning method. Its spectral properties, birefringence, and RI response were investigated. The Bragg resonance dip showed a linear RI response with sensitivities of 229 nm/RIU and 120 nm/RIU for high-order and fundamental modes within an RI range from 1.345 to 1.395. Additionally, this device provides a relatively weak response to ambient temperature changes. This novel μ-FBG design could have significant applications in biochemical sensing.

References

[1] Y. Tian *et al.*, "High performance magnetically controllable microturbines," *Lab chip*, vol. 10, no. 21, pp. 2902–2905, Nov. 2010.
[2] T. Y. Huang *et al.*, "3D printed microtransporters: Compound micromachines for spatiotemporally controlled delivery of therapeutic agents," *Adv. Mater.*, vol. 27, no. 42, pp. 6644–6650, Nov. 2015.
[3] M. Straub and M. Gu, "Near-infrared photonic crystals with higher-order bandgaps generated by two-photon photopolymerization," *Opt. Lett.*, vol. 27, no. 20, pp. 1824–1826, 2002.
[4] S. Kawata, H.-B. Sun, T. Tanaka, and K. Takada, "Finer features for functional microdevices," *Nature*, vol. 412, no. 6848, pp. 697–698, 2001.
[5] L. P. C. Gomez *et al.*, "Rapid prototyping of chemical microsensors based on molecularly imprinted polymers synthesized by two-photon stereolithography," *Adv. Mater.*, vol. 28, no. 28, pp. 5931–5937, Jul. 2016.
[6] L. Tong *et al.*, "Subwavelength-diameter silica wires for low-loss optical wave guiding," *Nature*, vol. 426, no. 6968, pp. 816–819, 2003.
[7] C. R. Liao, D.-N. Wang, Y. Li, T. Sun, and K. T. V. Grattan, "Temporal thermal response of type II-IR fiber Bragg gratings," *Appl. Opt.*, vol. 48, no. 16, pp. 3001–3007, Jun. 2009.
[8] X. Fang, C. R. Liao, and D. N. Wang, "Femtosecond laser fabricated fiber Bragg grating in microfiber for refractive index sensing," *Opt. Lett.*, vol. 35, no. 7, pp. 1007–1009, Apr. 2010.
[9] Y. Ran *et al.*, "193nm excimer laser inscribed Bragg gratings in microfibers for refractive index sensing," *Opt. Express*, vol. 19, no. 19, pp. 18577–18583, 2011.
[10] M. Ding, M. N. Zervas, and G. Brambilla, "A compact broadband microfiber Bragg grating," *Opt. Express*, vol. 19, no. 16, pp. 15621–15626, 2011.
[11] J. Wang *et al.*, "Bragg resonance in microfiber realized by two-photon polymerization," *Opt. Express*, vol. 26, no. 4, pp. 3732–3737, 2018.
[12] C. Liao *et al.*, "D-shaped fiber grating refractive index sensor induced by an ultrashort pulse laser," *Appl. Opt.*, vol. 55, no. 7, p. 1525, 2016.
[13] Y. Ran, L. Jin, L.-P. Sun, J. Li, and B.-O. Guan, "Bragg gratings in rectangular microfiber for temperature independent refractive index sensing," *Opt. Lett.*, vol. 37, no. 13, pp. 2649–2651, 2012.
[14] Y. Zhang *et al.*, "Refractive index sensing based on higher-order mode reflection of a microfiber Bragg grating," *Opt. Express*, vol. 18, no. 25, pp. 26345–26350, 2010.
[15] G. Brambilla *et al.*, "Optical fiber nanowires and microwires: Fabrication and applications," *Adv. Opt. Photon.*, vol. 1, no. 1, pp. 107–161, Jan. 2009.
[16] S. Maruo, O. Nakamura, and S. Kawata, "Three-dimensional microfabrication with two-photon-absorbed photopolymerization," *Opt. Lett.*, vol. 22, no. 2, pp. 132–134, 1997.
[17] C. Lin *et al.*, "Fiber surface Bragg grating waveguide for refractive index measurements," *Opt. Lett.*, vol. 42, no. 9, pp. 1684–1687, 2017.